LBL-37301
UC-414

Lawrence Berkeley Laboratory

UNIVERSITY OF CALIFORNIA

Physics Division

Presented at the First Arctic Workshop on Future Physics and Accelerators, Saariselka, Finland, August 22, 1994, and to be published in the Proceedings

Status of the SLAC/LBL/LLNL B-Factory and the BABAR Detector

P. Oddone

August 1994

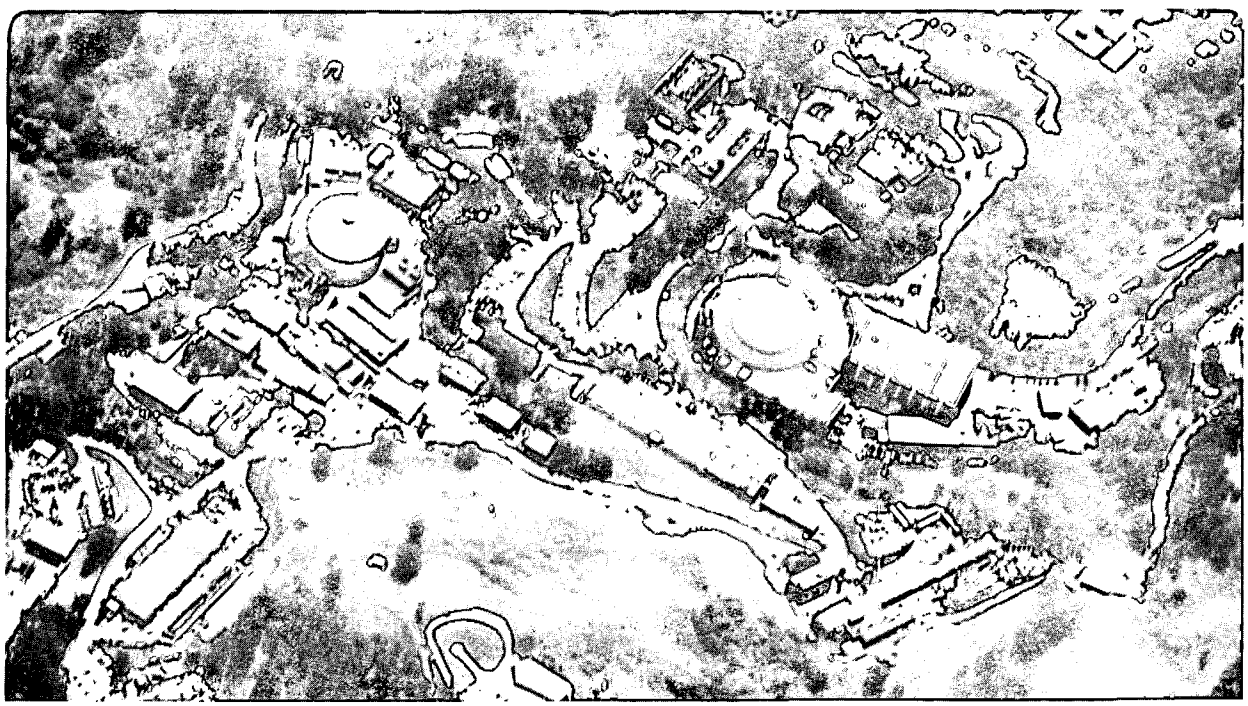

REFERENCE COPY
Does Not
Circulate
Bldg. 50 Library.
LBL-37301
Copy 1

Prepared for the U.S. Department of Energy under Contract Number DE-AC03-76SF00098

DISCLAIMER

This document was prepared as an account of work sponsored by the United States Government. While this document is believed to contain correct information, neither the United States Government nor any agency thereof, nor The Regents of the University of California, nor any of their employees, makes any warranty, express or implied, or assumes any legal responsibility for the accuracy, completeness, or usefulness of any information, apparatus, product, or process disclosed, or represents that its use would not infringe privately owned rights. Reference herein to any specific commercial product, process, or service by its trade name, trademark, manufacturer, or otherwise, does not necessarily constitute or imply its endorsement, recommendation, or favoring by the United States Government or any agency thereof, or The Regents of the University of California. The views and opinions of authors expressed herein do not necessarily state or reflect those of the United States Government or any agency thereof, or The Regents of the University of California.

This report has been reproduced directly from the best available copy.

Lawrence Berkeley Laboratory is an equal opportunity employer.

DISCLAIMER

This document was prepared as an account of work sponsored by the United States Government. While this document is believed to contain correct information, neither the United States Government nor any agency thereof, nor the Regents of the University of California, nor any of their employees, makes any warranty, express or implied, or assumes any legal responsibility for the accuracy, completeness, or usefulness of any information, apparatus, product, or process disclosed, or represents that its use would not infringe privately owned rights. Reference herein to any specific commercial product, process, or service by its trade name, trademark, manufacturer, or otherwise, does not necessarily constitute or imply its endorsement, recommendation, or favoring by the United States Government or any agency thereof, or the Regents of the University of California. The views and opinions of authors expressed herein do not necessarily state or reflect those of the United States Government or any agency thereof or the Regents of the University of California.

LBL-37301
UC-414

Status of the SLAC/LBL/LLNL B-Factory and the BABAR Detector

Pier Oddone

Physics Division
Lawrence Berkeley Laboratory
University of California
Berkeley, California 94720

August 1994

This work was supported by the Director, Office of Energy Research, Office of High Energy and Nuclear Physics, Division of High Energy Physics, of the U.S. Department of Energy under Contract No. DE-AC03-76SF00098.

STATUS OF THE SLAC/LBL/LLNL B-FACTORY AND THE BABAR DETECTOR*

PIER ODDONE
Physics Division, Lawrence Berkeley Laboratory, 1 Cyclotron Road
Berkeley, CA 94720, USA

ABSTRACT

In this paper we briefly describe the physics reach of the SLAC/LBL/LLNL Asymmetric B-Factory, the progress on the machine design and construction, the progress on the detector design, and the schedule to complete both projects.

1. Physics Reach

The primary motivation of the Asymmetric B-Factory is the study of *CP* violation. The decay of B mesons and, in particular, the decay of neutral B mesons, offers the possibility of determining conclusively whether *CP* violation is part and parcel of the Standard Model with three generations of quarks and leptons. Alternatively, we may discover that *CP* violation lies outside our present framework.

Many different B decay modes can be studied in the B-Factory. The asymmetries observed in these decay modes can be related, in many instances without additional corrections, to the underlying parameters of the CKM matrix. In fact, the observed asymmetries may be the only precise way to determine some of the CKM matrix elements.

The measurement of *CP* asymmetry is basically a counting experiment: the number of decays of a given type are counted as a function of the separation of the two B mesons, one decaying to the state of interest and one decaying to a tagging state. The tagging state is a state that determines whether the tagging B is a particle or an antiparticle. The asymmetry is then constructed by comparing the particle and antiparticle tagged rates.

It has become customary to describe the measurements of *CP* asymmetries in terms of the angles of the unitarity triangle. The unitarity triangle is simply a graphical representation of the unitarity of the CKM matrix. It turns out that the *CP* asymmetries in various decay channels are simply related to the interior angles of the unitarity triangle, as shown in Figure 1. The different decay modes of neutral B mesons measure different angles of the unitarity triangle. Table 1 shows the expected physics reach with an integrated luminosity of 30 fb^{-1} in terms of the errors in the angles of the unitarity triangle. This is the integrated luminosity expected in one year of running.

*This work was supported in part by the United States Department of Energy, contract number DE-AC03-76SF00098, and other DoE contracts.

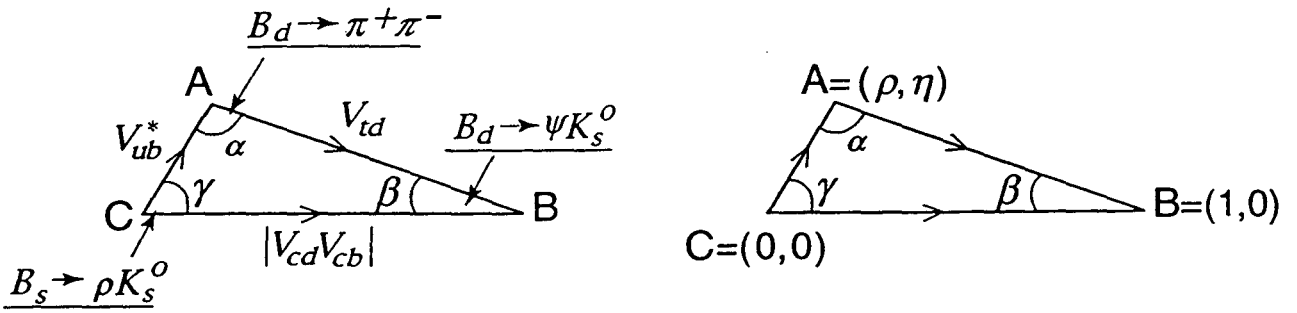

Figure 1: The unitarity triangle. The parameters ρ and η are from the Wolfenstein parameterization of the CKM matrix.

Table 1: How well do we measure angles? The answer depends on a detailed simulation of modes. For the present BABAR:

Mode	Br	Background signal	Measured quantity error	Comments
ψK_s	4×10^{-4}	0	δ (sin2β) = 0.13	very clean interpretation
ψK^{*0}	1.2×10^{-3}	0	δ (sin2β) = 0.20	very clean interpretation
D^+D^-	6×10^{-4}	~.1	δ (sin2β) = 0.20	clean interpretation
$D^{*+}D^{*-}$	1.5×10^{-3}	~.1	δ (sin2β) = 0.16	clean interpretation
Σ			δ (sin2β) = 0.09	
$\pi^+\pi^-$	2×10^{-5}	.1	δ (sin2α) = 0.24	penguin contamination?
$\rho^\pm\pi^\mp$	8×10^{-5}	.1	δ (sin2α) = 0.12	penguin contamination?
Σ			δ (sin2α) = 0.11	

For $\int \mathcal{L}$ dt = 30 fb^{-1} (= 1 nominal year)

The sides of the triangle can also be measured, albeit with considerable uncertainty arising partly from experimental and partly from theoretical reasons. Figure 2 shows the region of allowed angles, given the present knowledge of the sides of the triangle and various assumptions about the bag constants and the decay constants for B and K mesons. The sides of the triangles themselves will be better measured at the B-factory because the greater statistics available both decreases statistical uncertainty and opens up new methods for determining the relevant matrix elements.

Figure 3 is a possible example of the situation after three years of running and 100 fb^{-1} of data. In this imaginary example, the measurements of the sides of the triangle have progressed to the point where only a narrow region of angles is allowed. The measured angles also define a narrow but different and distinct region, indicating the inconsistency of the Standard Model and the need for new understanding.

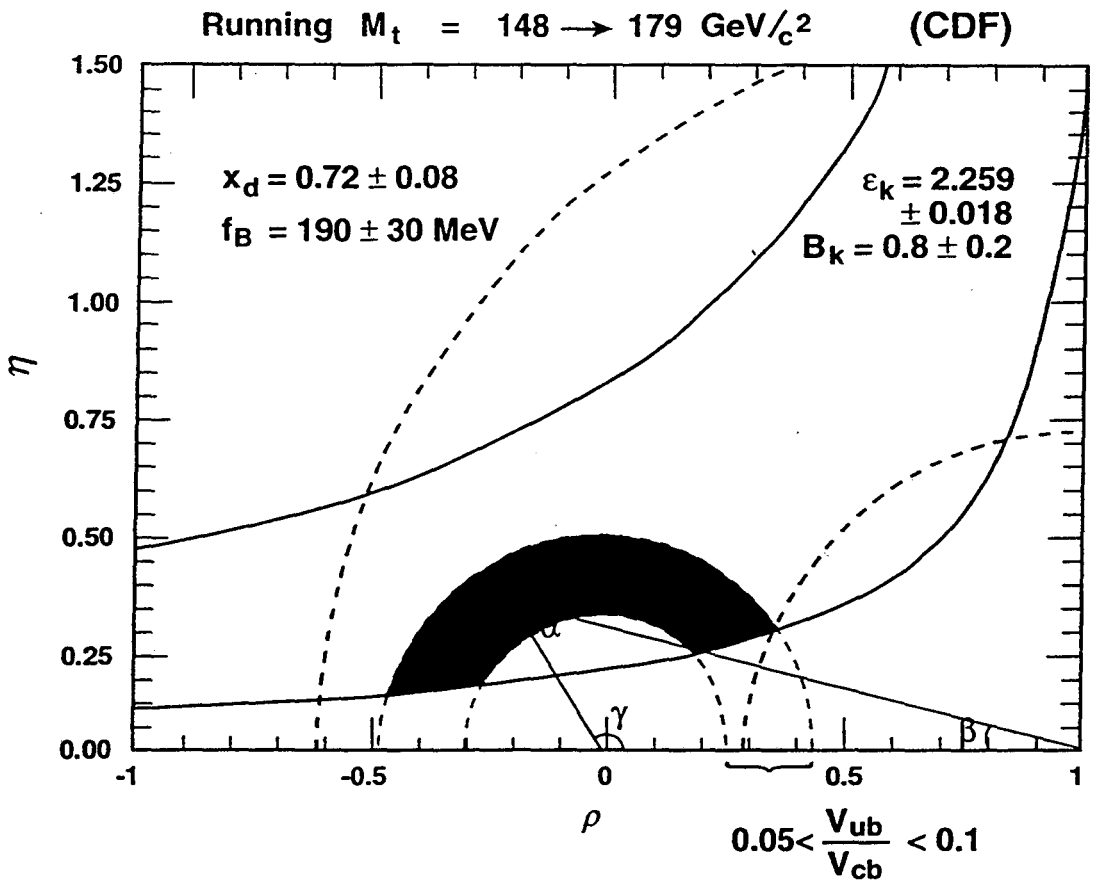

Figure 2: Region of allowed angles for the unitarity triangle, given stated assumptions.

2. Progress in the Accelerator Design and Construction

The idea of an Asymmetric B-Factory can be realized relatively economically at SLAC, where a powerful injector, an existing tunnel, and a ring of magnets suitable for the high energy ring already exist. The requirements for the accelerator are, however, very challenging.

The machine design aims to maximize the luminosity. For two unequal-energy rings the luminosity formula is given by:

$$\mathcal{L} = 2.17 \times 10^{34} \xi (1 + r) \frac{I \cdot E}{\beta_y^*} \quad [\mathrm{cm}^{-2}\mathrm{s}^{-1}]$$

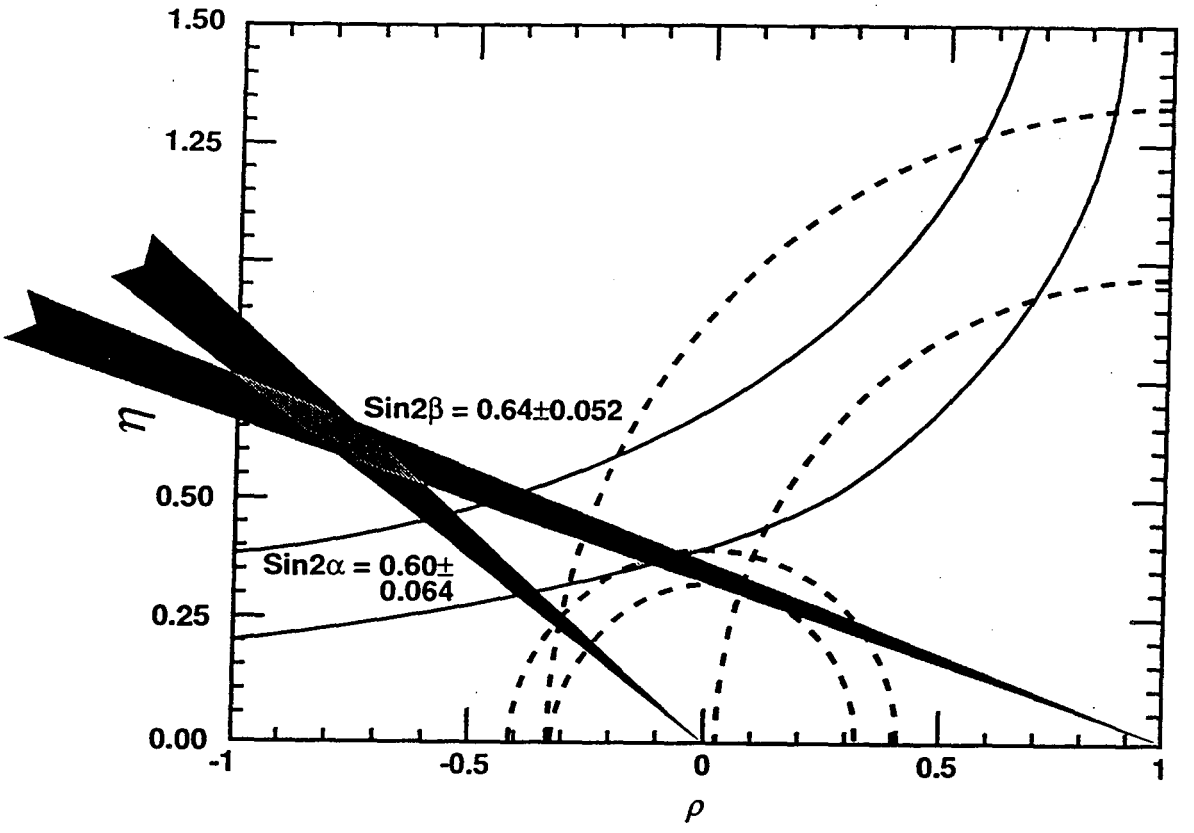

Figure 3: Prospects of determining the consistency with the Standard Model. Assumptions: $m_t = 175 \pm 5$ GeV/c^2, $V_{cb} = 0.037 \pm 0.001$, $f_B = 170 \rightarrow 210$ MeV, $x_d = 0.70 \pm 0.01$, $\frac{V_{ub}}{V_{cb}} = 0.08 \pm 0.01$, $B_k = 0.7 \rightarrow 0.9$.

where

I	=	total current [A]
β_y^*	=	vertical beta function at IP [cm]
r	=	aspect ratio (σ_y/σ_x) (detector constraint)
E	=	beam energy [GeV] (physics constraint)
ξ	=	$\Delta\nu_{bb,max}$ (accelerator physics constraint)

and the values can be taken from either ring. There is a fundamental limit due to the beam-beam interaction that constrains ξ to values less than 0.06. Practical requirements in the design of the interaction region preclude the use of round beams so that the parameter r is effectively set to zero in the equation above. The only two parameters left to maximize the luminosity are the current I and the focusing function β_y^*. So the name of the game is to try to maximize the current I while trying to minimize β_y^*. The design logic that follows from this strategy is depicted graphically in Figure 4. Fundamental to the design approach is to have the parameters of a single bunch-bunch collision be no different from those in operating machines. This implies

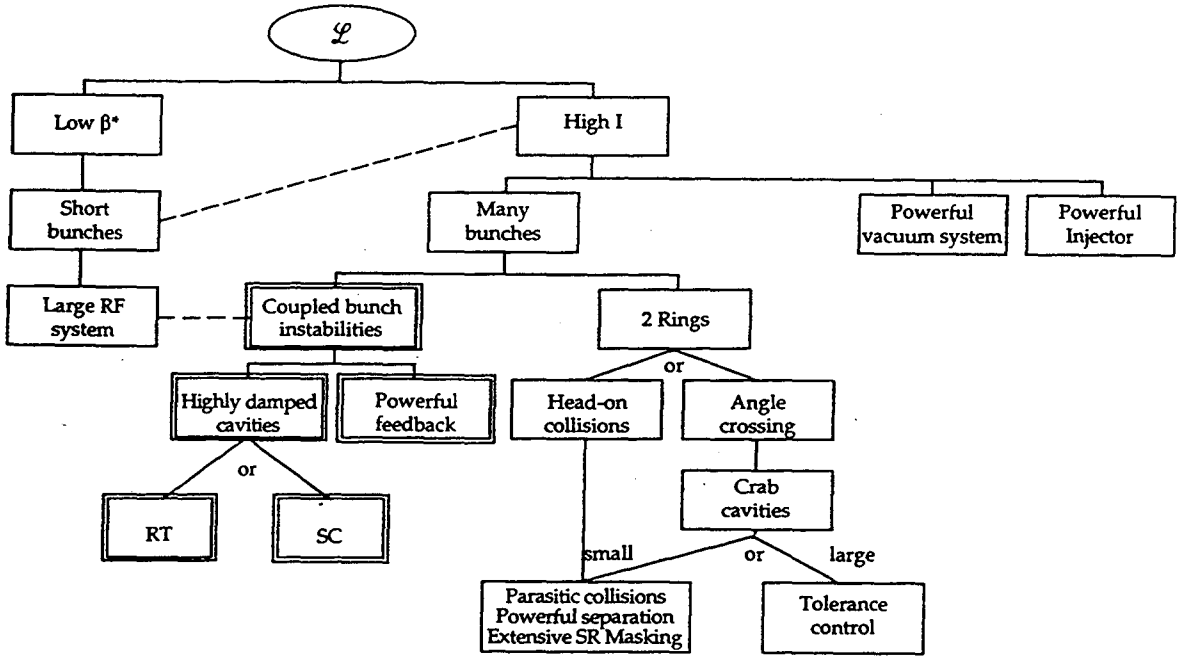

Figure 4: Design logic for the accelerator.

that the increased current must be achieved by having many bunches circulating in each ring.

The solid lines in the figure depict the major design drivers, while the dashed lines show the weaker drivers. In minimizing the focusing function β_y^*, one typically increases the total RF voltage around the ring to create a stronger focusing in the longitudinal direction, and thus a shorter bunch (there is no point in having a β_y^* smaller than the length of the bunch). The large RF voltage typically means many cavities which, coupled with the large currents and large number of bunches, lead to potential multi-bunch instabilities. The many bunches also require a special separation system at the interaction point in order to avoid parasitic crossings.

The most critical design choices revolve around the control of multi-bunch instabilities and the beam separation scheme. For the SLAC/LBL/LLNL B-Factory, the choice is specially damped conventional cavities with a powerful feedback system for the control of multi-bunch instabilities. For the separation scheme, a dipole magnet is chosen near the interaction point, allowing for the beams to collide head-on as in present accelerators. With these choices, one arrives at the parameters shown in Table 2.

In the following sections we describe very briefly the various parts of the acceler-

Table 2: PEP-II main collider parameters.

	LER	HER
Energy, E [GeV]	3.1	9
Circumference, C [m]	2199.32	2199.32
ϵ_y/ϵ_x [nm · rad]	2.6/64	1.9/48
β_y^*/β_x^* [cm]	1.5/37.5	2.0/50.0
ξ	0.03	0.03
f_{RF} [MHz]	476	476
V_{RF} [MV]	5.9	18.5
Bunch length, σ_ℓ [mm]	10	10
Number of bunches, κ_B	1658^+	1658^+
Bunch separation, S_B [m]	1.26	1.26
Damping time, τ_E/τ_x [ms]	19.8/40.3	18.4/37.2
Total current, [A]	2.14	0.99
U_0 [MeV/turn]	1.14	3.58
Luminosity, $\mathcal{L}$ [$\mathrm{cm}^{-2}\mathrm{s}^{-1}$]	3×10^{33}	3×10^{33}

ator and their status. For a more comprehensive review of the machine, we refer the reader to the PEP II Conceptual Design Report[1].

2.1. Injector

The developments that have occurred on the SLC at SLAC have provided a linac with high current, low emittance, and a very high level of beam dynamics control. This linac makes an ideal injector for the B-factory. We expect that, starting from scratch, it will be possible to fill the two rings, producing two amperes of current in the Low Energy Ring and one ampere of current in the High Energy Ring, in about six minutes. The more common "top up" mode, in which the beams are brought to full current starting from the residual currents at the end of the fill, should take about three minutes. This feature of rapid injection is essential if the B-Factory is truly going to operate as a factory.

To optimize the injection, the beams of positrons and electrons will be taken from the linac at the appropriate points to yield "at energy" injection and will be delivered to PEP II by a new transfer line. The beam transfer line quadrupoles have been prototyped and tested and are now in full production.

2.2. High Energy Ring (HER) magnets

The magnets for the HER are largely recycled magnets from the old PEP ring. These magnets have been removed from the PEP tunnel, tested, and measured and are being reconditioned. They will be replaced in the tunnel in a configuration very

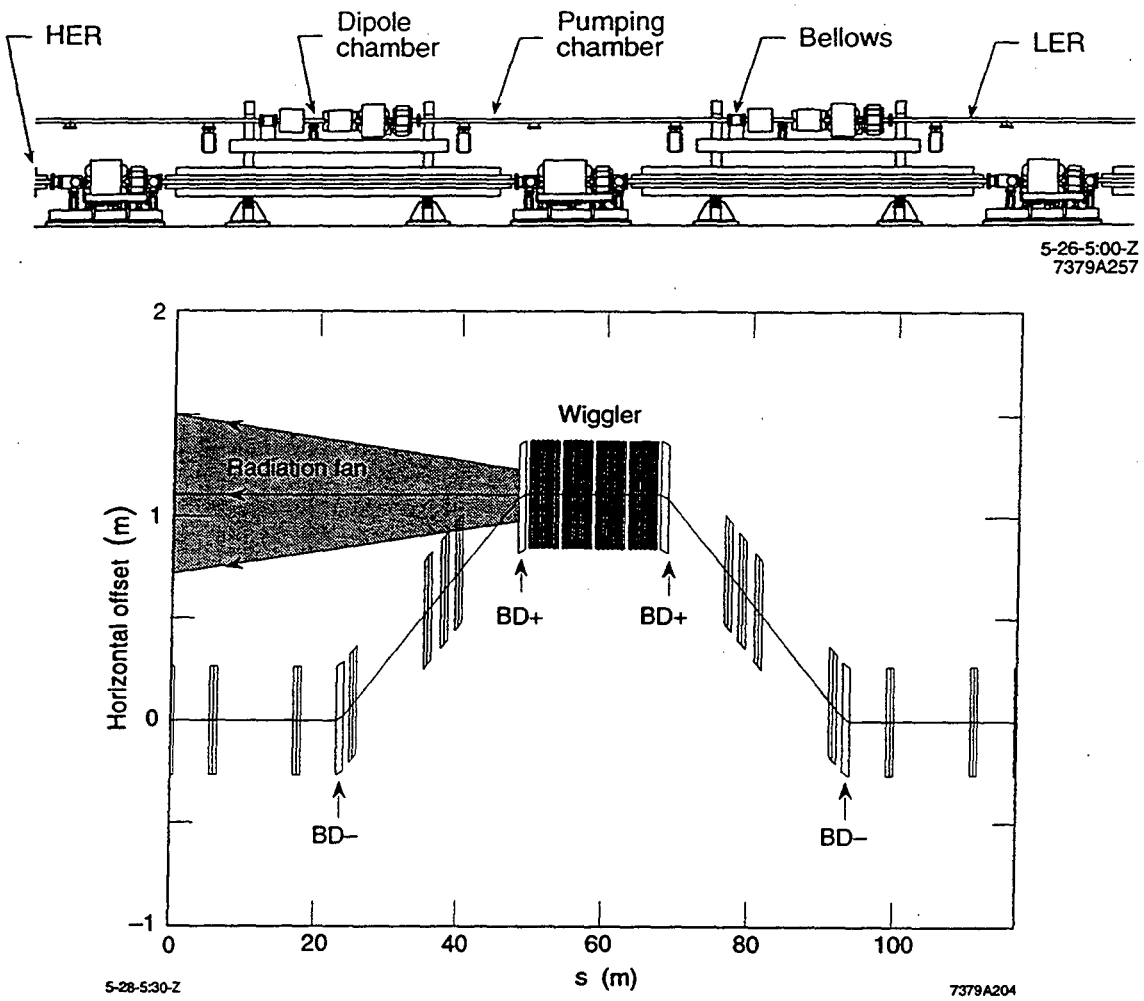

Figure 5: Low Energy Ring features.

similar to the old PEP ring, with 96 FODO cells and six long straight sections. The injection into the HER is in the vertical plane to avoid parasitic crossing issues. The modular design of the lattice provides for independent emittance, tune, and injection control.

2.3. Low Energy Ring (LER) magnets

The LER is an entirely new ring, to be physically located above the HER. Since the radi of the two machines are the same, but the energies very different, there is a problem in matching the emittances of the two rings. To accomplish this there are two special features of the LER: the dipole magnets are short and of high field, and wiggler magnets are also included in the lattice to increase the synchrotron radiation excitation and decrease the damping time. Figure 5 shows the typical arrangement of the wiggler magnets in the LER. At this point all magnets have been designed, and the procurement process for the magnets has started.

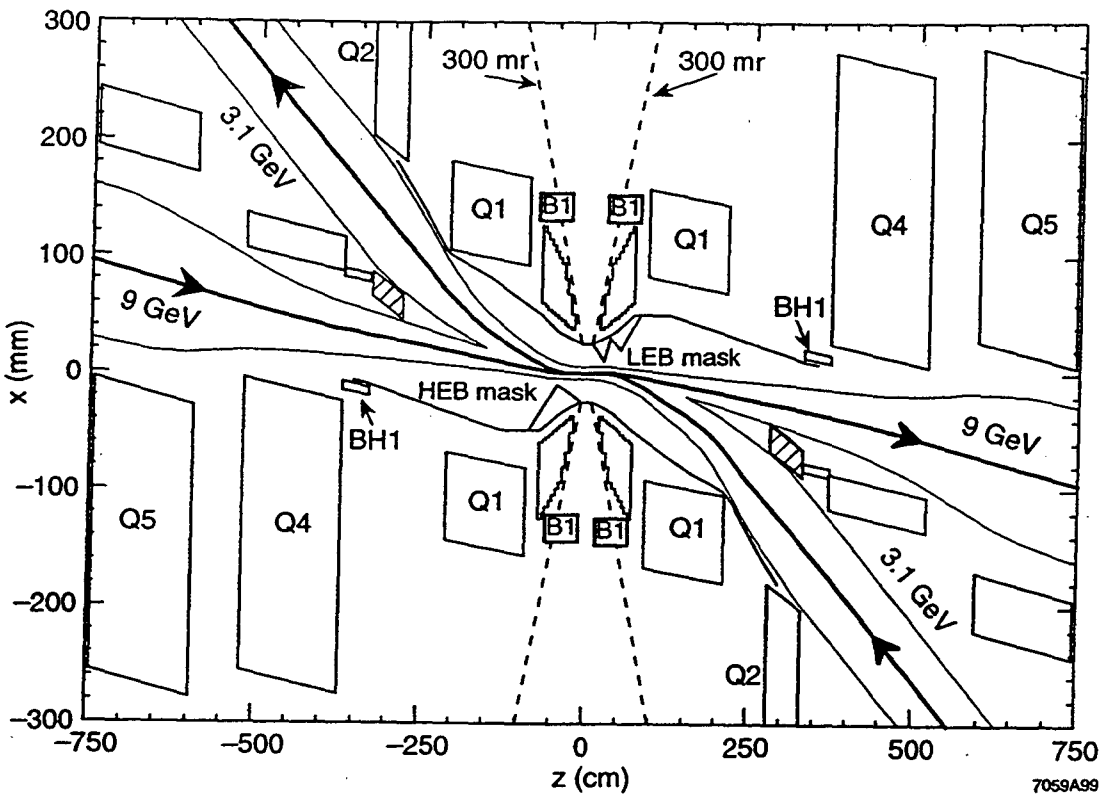

Figure 6: Quadrupoles (Q) and bending magnet (B1) near the interaction point.

2.4. Vacuum system

The relatively large bending radius of the existing PEP ring makes the vacuum requirements manageable. The most stringent requirements are on the HER, where an extruded copper vacuum chamber is used. Copper experiences less desorption under synchrotron radiation than does aluminum. The copper chamber has an antechamber with distributed ion pumps. Lumped ion pumps are also used.

The LER uses special beam stops for the synchrotron radiation produced by the wigglers. Otherwise, the chamber is a conventional aluminum chamber.

The interaction region requires special handling, as the conductance of the small chamber is low and the region is very crowded with synchrotron radiation masks, close-in magnetic elements, and the detector itself. The detailed design of this region has started but is not complete. Figure 6 shows a schematic diagram of this complex area.

2.5. Radio frequency system

The RF system must handle large beam currents while minimizing beam instabilities due to multi-bunch interactions. The instabilities are driven by higher-order modes (HOMs) in the cavities, so a special highly damped cavity has been designed. A prototype of this cavity has been tested at low power and has shown satisfactory performance. A cavity suitable for full power tests is under fabrication and should be available by the end of the year.

To damp HOMs, three small waveguides are attached at strategic places in the cavity. The HOMs "leak" out of the cavity and are absorbed in ferrite cores at the end of the special waveguides. Figure 7 shows how a completed cavity will appear in the PEP II machine.

2.6. Feedback system

Even with the specialized HOM damping of the RF cavities, some multi-bunch instabilities build up faster than the damping, owing to synchrotron radiation. To control the growth of these instabilities, a powerful feedback system is required. Special electrodes sense the position of each bunch. A set of fast digital processors determines the required feedback "kick," which is then delivered to each bunch by a set of transverse and longitudinal electrodes. This system has been prototyped and tested at the Advanced Light Source (ALS) at LBL with satisfactory performance. The currents at the ALS are typically 0.4 amperes at 1.2 GeV.

2.7. Interaction region

One of the most complex parts of the machine is the interaction region. In particular, the choice of head-on collisions implies that powerful bending magnets need to placed closed to the interaction point (IP) to separate the two beams. Optical components near the interaction area need to handle both beams. Near the IP both beams pass through the same components. As the beams start to separate, the components have to provide two channels. This leads to very complex magnet design, as is illustrated in Figure 8, which shows the Q2 septum magnet. This magnet provides focusing for the high energy beam but lets the low energy beam pass through unaffected.

3. The BABAR detector

In the Asymmetric B-Factory, only one interaction region will be developed. There are several reasons for this. First and foremost is the expectation that the machine will be easier to operate and more reliable with only one interaction point. Second is the observation that the machine may have a higher luminosity with only one collision point, since a second collision would add toward the tune shift limit. Finally, so much is known about the typical event configuration that the detector design typically

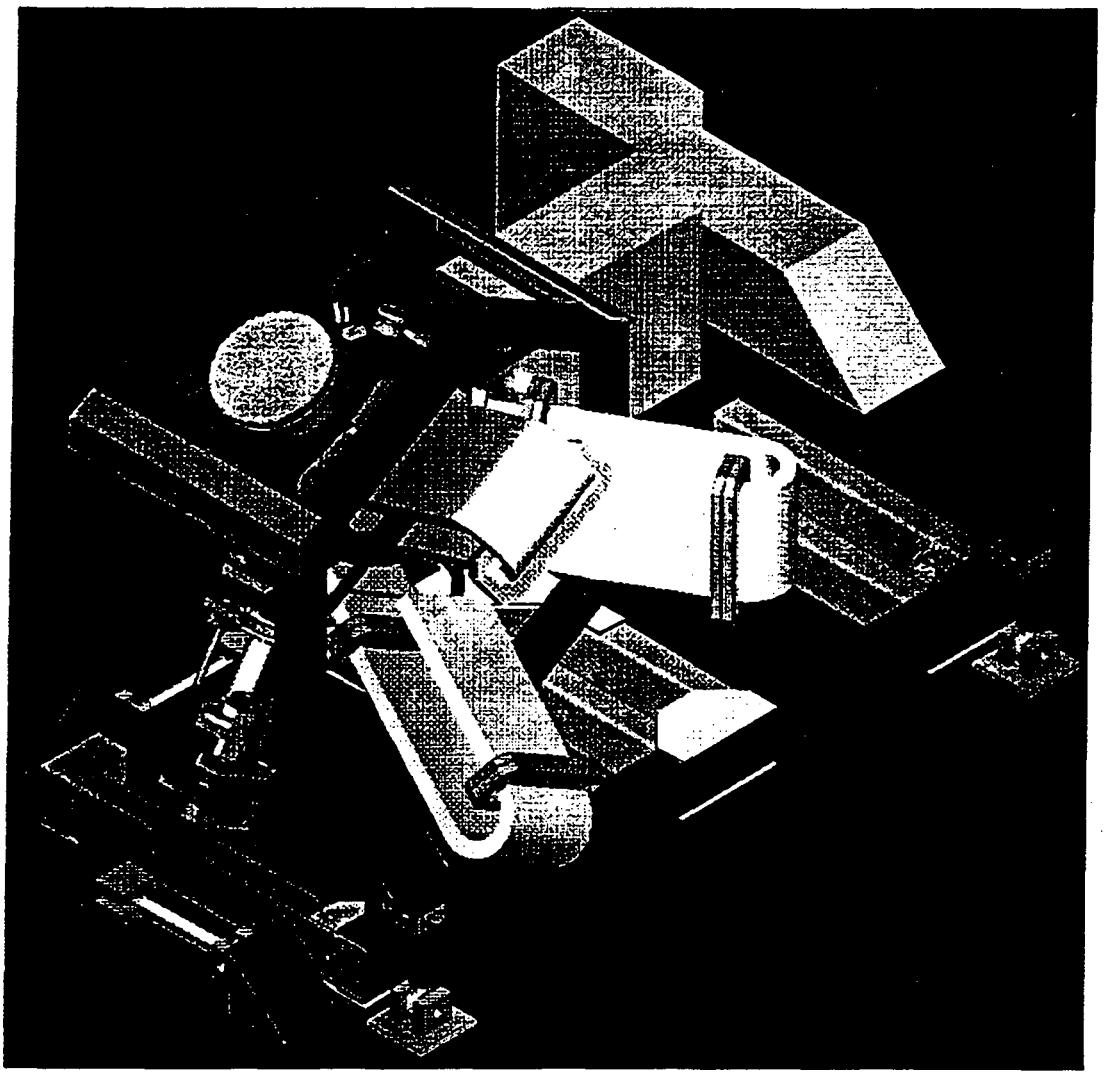

Figure 7: RF cavity for PEP II.

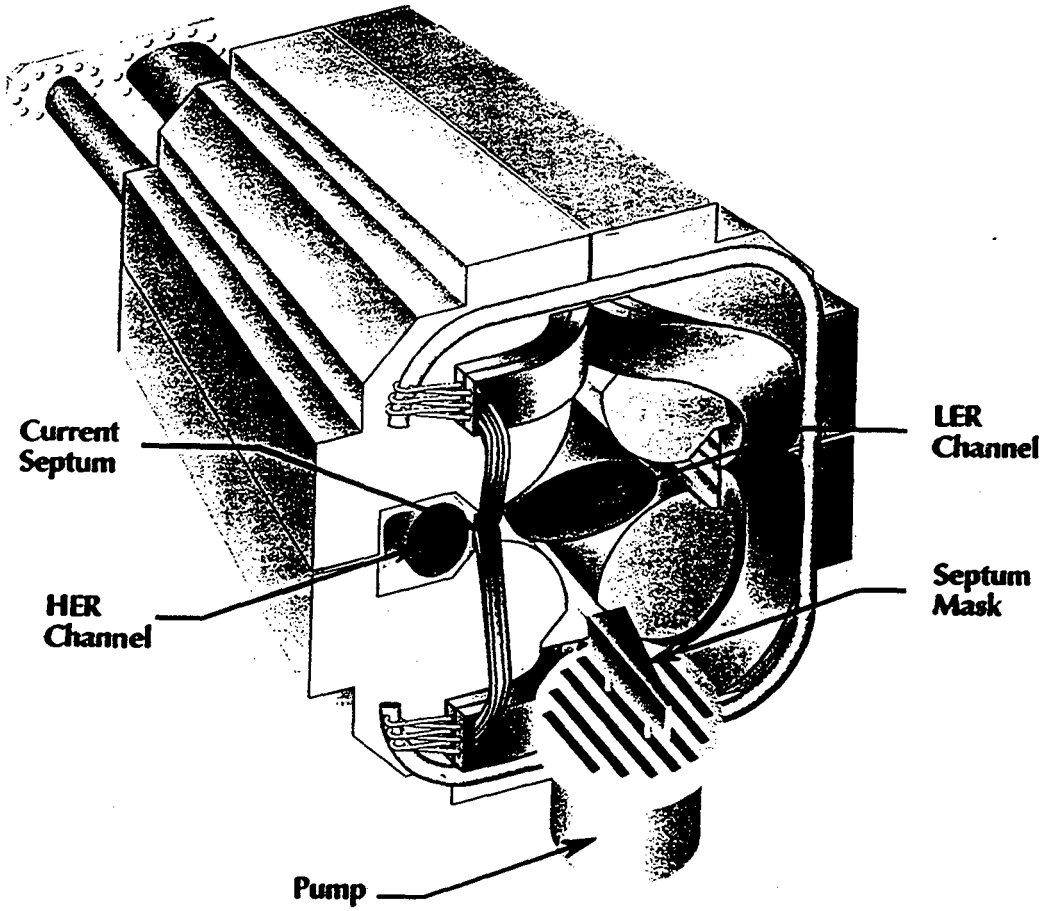

Figure 8: Septum quadrupole Q2 near the interaction region.

converges to approximately a single design as the BABAR and BELLE detectors appear to be demonstrating.

3.1. The collaboration

Starting late last fall, a large international collaboration has formed to develop the detector for the PEP II B-Factory. Eventually the collaboration adopted the BABAR name for the detector. Last June, the collaboration was formalized with the submission of a Letter of Intent (LOI) to SLAC. The 75 institutions that signed the LOI are shown in Table 3. The collaboration received first stage approval in July 1994 and is proceeding to develop a Technical Design Report to be published in the spring of 1995. Many, but not all, technical choices have been made. In the following paragraphs, we describe briefly the status of the detector design. At this stage, the principal design choice remaining is the particle identification system. For

Table 3: The BABAR collaboration. Numbers in brackets represent the number of institutions followed by the number of collaborations.

US [29/206]
California Institute of Technology
UC, Davis
UC, HRPA
UC, Irvine
UC, Los Angeles
UC, Santa Barbara
UC, Santa Cruz
U of Cincinnati
U of Colorado
Colorado State U
U of Houston
U of Iowa
Iowa State U
LBL
LLNL
U of Maryland
U of Massachusetts
MIT
U of Mississippi
Mount Holyoke College
U of Notre Dame
ORNL/Y-12
U of Pennsylvania
Princeton
Rutgers
SLAC
U of Texas at Dallas
Vanderbilt
U of Wisconsin

Canada [7/22]
U of British Columbia
Carleton U and CRPP
McGill U
U de Montréal
TRIUMF
U of Victoria
York U

China [4/19]
Beijing Glass Research Inst.
Inst. of High Energy Physics, Beijing
Shanghai Inst. of Ceramics (SICCAS)
Tsinghua U, Beijing

France [6/37]
LAPP, Annecy
LAL Orsay
Ecole Polytechnique
U Pierre et Marie Curie, Paris 6
Collége de France
CEA, DAPNIA, CE-Saclay

Germany [2/7]
Technische U Dresden
U Karlsruhe

Italy [12/49]
INFN, Bari and U di Bari
INFN, Ferrara
Lab. Nazionali di Frascati dell' INFN
INFN, Genova and U di Genova
INFN, Milano and U di Milano
INFN, Napoli and U di Napoli
INFN, Padova
U di Pavia
INFN, Pisa, U di Pisa and Scuola Normale
INFN, Superiore di Sanita', Roma
INFN, Torino and U di Torino
INFN, Trieste and U di Trieste

Russia [2/40]
Budker Institute, Novsibirsk
JINR, Dubna

United Kingdom [10/30]
U of Bristol
Brunel University
U of Edinburgh
U of Lancaster
U of Liverpool
Imperial College
Queen Marry & Westfield College
Royal Holloway & Bedford New College
U of Manchester
Rutherford Appleton Laboratory

Taiwan [2/4]
Academia Sinica, Taiwan
National Taiwan U, Taiwan

a more detailed description of the detector, please refer to the LOI[2].

3.2. Overall considerations in the design of BABAR

The requirements on the detector are very demanding. Charged particles need to be tracked and measured with great precision to allow for clean reconstruction of exclusive charged final states. Many final states of interest have π^0s, such as the state $\rho\pi$, requiring that photons be measured with good energy and spatial resolution. Particles also need to be identified, since kinematics separation cannot distinguish the substitution of a pion for a kaon in the final state. This particle identification needs to be done over almost the entire kinematic range, because kaons used for tagging span the full momentum spectrum. At the high end of the momentum spectrum, we want to separate two-body decays such as $\pi\pi$ and $K\pi$. Muon identification is also important, as muons are used in the tagging. Finally, the separation of the two B decay vertices needs to be made with a resolution below 100 micrometers to measure the time evolution on which the CP asymmetry measurement hinges. All of this has to be done with a finite budget.

Figure 9 shows the overall picture of the detector. Starting from the vertex, particles go through a thin beam pipe, then the vertex detector, a drift chamber, and particle identification system before reaching a CsI crystal calorimeter. All of the above elements are contained in a 1.5-tesla superconducting solenoid. Outside the solenoid lies the muon identifier, consisting of iron plates to return the magnetic flux and chambers interspersed with the iron plates. In the sections below we give a thumbnail sketch of each system.

3.3. Vertex detector

The vertex detector consists of five layers of double-sided silicon strips. Strips have a 50-micrometer pitch. Every other strip is read, with strips left floating between those that are read out. The detector has all the electronics outside the tracking volume, along the end cones shown in Figure 10. The innermost detector planes are cylindrical, while the outer ones have a more complicated shape in order to minimize multiple scattering. The detector wafers are mounted on "bridges," and the strips are connected with micro bonds across the "break." The resolution simulated for the detector is well below the required 100 micrometers. One goal of the vertex detector is to provide stand-alone tracking for low-energy tracks that are either unmeasured or poorly measured in the drift chamber.

3.4. Drift chamber

The drift chamber is of a low-mass design, using a helium-isobutane gas mixture. It is presently debated whether the chamber should have only stereo layers (two directions) or both stereo and axial layers. The advantage of the all-stereo design is that all cells are identical and the chamber is effectively homogeneous. The combined

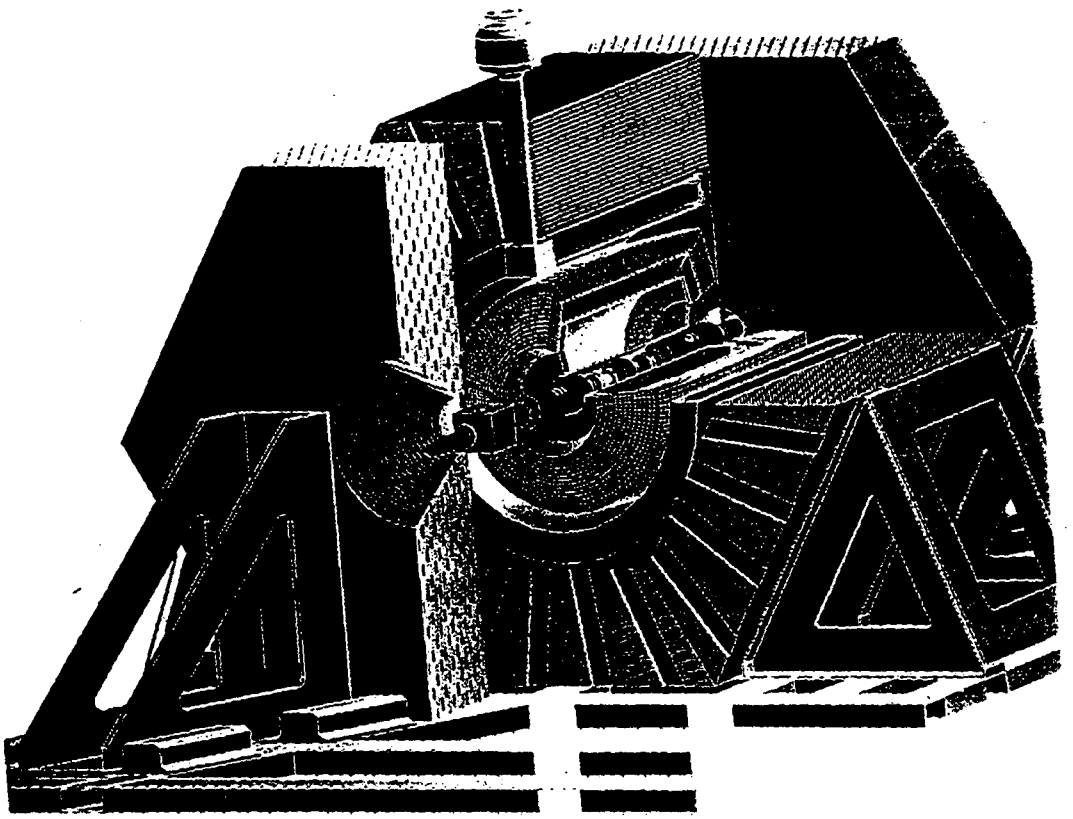

Figure 9: Overall view of the BaBar detector.

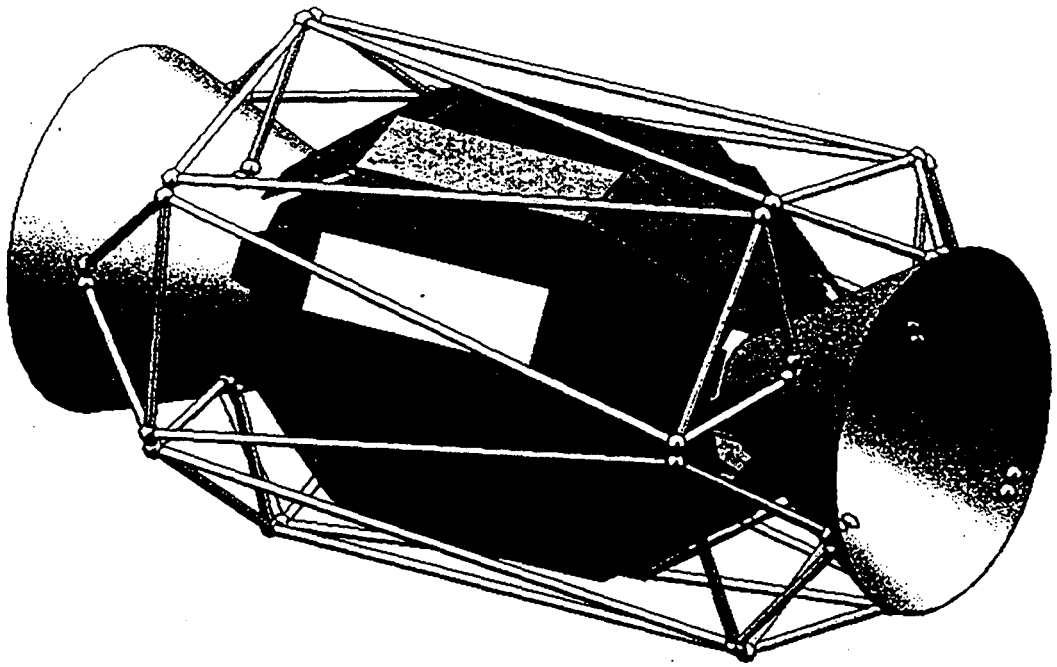

Figure 10: The BABAR vertex detector.

axial/stereo design offers easier track reconstruction but requires special cells at the transition between axial and stereo layers. The resolution achieved by this design is $\sigma = 0.03$ GeV/c at 1 GeV/c momentum for central tracks. A prototype chamber has been built and is currently under test.

3.5. Particle identification system

At this moment, three particle identification systems are being considered. All are variations of Cerenkov counters placed to surround the drift chamber.

The first system is based on a Fast RICH. The particles radiate in a radiator layer consisting of a liquid radiator enclosed in a quartz box. The radiated photons strike a photocathode surface made by depositing CsI on an appropriate substrate. The photoelectrons liberated at the surface are then multiplied in a conventional wire chamber. The cathode plane is segmented into pads in order to read out the position of the photoelectrons. The radius of the photoelectron ring determines whether the particle is a pion or a kaon. A small prototype detector has been built and tests are underway.

The second system is based on two layers of aerogel threshold Cerenkov counters. The first layer, appropriate for higher momenta, consists of blocks of aerogel with an index of refraction of 1.008. In the second layer, smaller blocks with an index of refraction of 1.06 are used for the lower momenta. The aerogel is enclosed in aluminum boxes painted with highly reflecting paint. Also, a wavelength shifter is coated onto the painted surface to extend the scattering length for photons. The light from the aerogel is viewed with fine-mesh phototubes or other suitable photo detectors, capable of operating in a 1.5-tesla magnetic field. Tests are scheduled to be performed at CERN during this fall.

The third system in contention is depicted in Figure 11. It consists of an imaging Cerenkov counter where the image is transmitted down quartz bars which are also the radiator medium. Transmission through the bars preserves the Cerenkov angles. These angles are read out on an imaging plane consisting of almost 15,000 phototubes. This special Cerenkov counter, called a DIRC, has been tested with cosmic rays and shows, in principle, satisfactory performance for π/K separation (greater than 4 sigma over the entire kinematic range). Because the bars extend all the way out of the detector, the DIRC presents special mechanical problems which are being studied.

A decision on what system to use is expected by the fall of 1994.

3.6. Calorimeter

The requirement to reconstruct $\pi^0 s$ over as broad a momentum range as possible leads to the selection of a thallium-doped CsI crystal calorimeter. The calorimeter consists of a barrel with approximately 7300 trapezoidal crystals and two endcaps with 2700 crystals. To optimize performance and cost, the depth of the calorimeter ranges from 18 X_0 to 15 X_0, depending on the angular region of the calorimeter. Several readout schemes are being tested. One involves two photodiodes directly reading the back of the crystal. A second uses a fluorescent flux concentrator (FFC) to cover the full back face of the crystals. The FFC is a wavelength shifter and collector, and it is read out by two photodiodes along its edges. This latter scheme uses smaller photodiodes than the direct readout. The aim of the readout system is to maximize signal to noise. A somewhat improved performance over present detectors is, in principle, possible if the low noise observed in prototype tests can be maintained for the full system. A lower noise also allows more crystals to be added, lowering the energy threshold for showers.

3.7. Magnet

The solenoid is of a relatively thin design and provides a uniform magnetic field over the tracking elements. The flux is returned by an iron flux return that is instrumented for muon detection as described below. The superconducting solenoid and cooling system adopts a number of techniques well-proven in magnets currently in use.

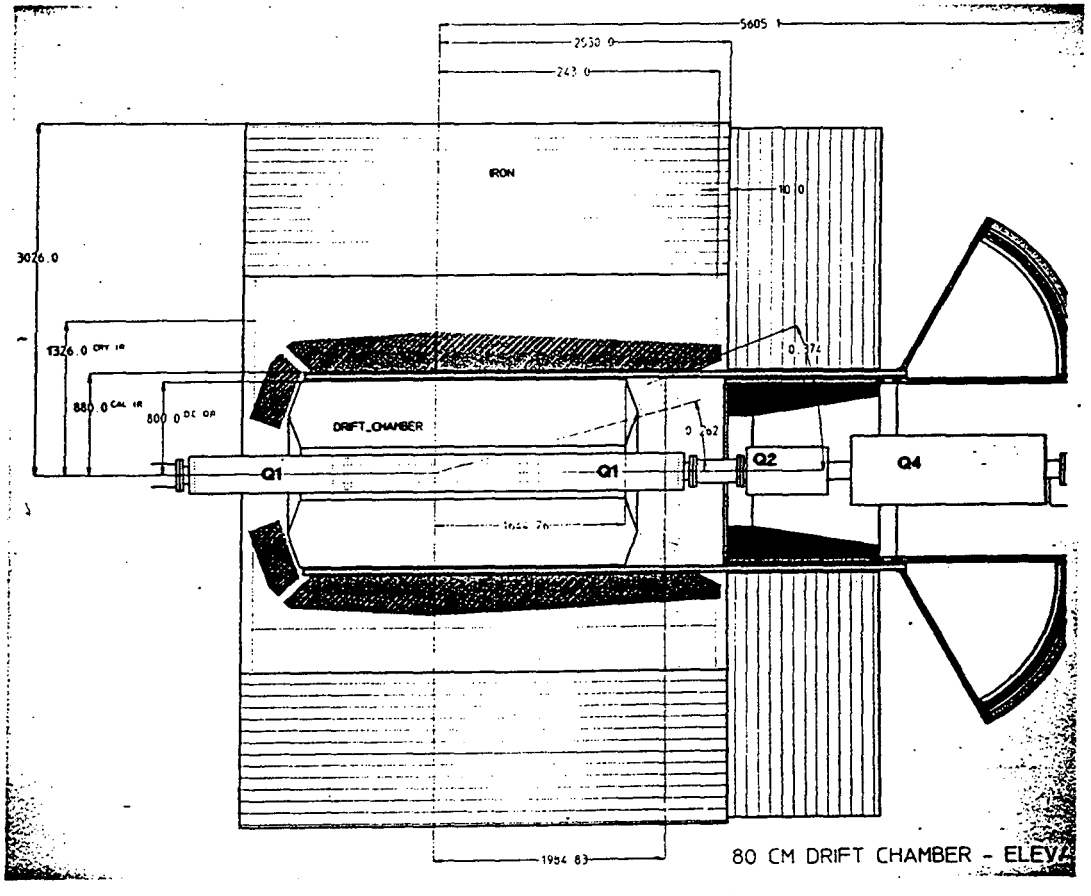

Figure 11: The DIRC counter shown in the forward regions of the detector.

3.8. Instrumented flux return

The iron flux is segmented into 2.5-centimeter slabs, and position-sensitive chambers are inserted in the gaps between the slabs. Over twenty layers of steel provide a fine segmentation and the ability to detect both muons and neutral hadrons. There are at least two types of detectors under contention. One is based on resistive plate chambers (RPCs) and another plasma streamer tubes (PSTs). A decision between these two types of detectors will also be made this fall. Simulations show that between 500 and 1000 GeV/c more than 90% of the muons will be detected and identified, with only a few percent pion contamination.

3.9. Electronics and trigger

The electronics and the trigger system are fully pipelined in order to minimize dead time for the system. The trigger rate is expected to be dominated by background.

This situation is necessary to insure nearly full efficiency for the events of interest. The triggers are formed from the combination of two primary triggers: a calorimeter trigger and a tracking trigger. The trigger system is organized in three levels. Level 1 has a maximum rate of 10 kHz to accommodate higher than expected backgrounds. The expected rate for interesting events arising from e^+e^- collisions is 30 Hz. The Bhabha event rate is 100 Hz. The expected background rates are 300 Hz. The system is designed to accommodate 30 times the expected background rate without loss of efficiency. Under all conditions, the rate of event building in Level 2 will be kept to less than 1 kHz, while the event rate to tape will be at most 0.1 kHz.

4. Schedule for the Accelerator and the Detector

The accelerator construction was announced in the fall of 1993, and construction started in 1994. The HER is mostly built by recycling the old PEP machine, and consequently it is completed early, along with the injection lines. By the fall of 1997 the HER will be tested with beam. The LER will be completed by mid 1988, and following a six months commissioning period, the machine should be available for experiments at the beginning of 1999.

The detector has had a slower start. The collaboration formed only at the end of 1993, and has spent this year designing the detector. A letter of intent (LOI) was approved by the laboratory in July 1994. This is being followed by a Technical Design Report that will be reviewed first by SLAC and then by the Department of Energy. Only after these reviews are completed, by the end of April 1995, will the detector fabrication officially start.

The detector schedule is very tight. If all develops smoothly, the detector will be completed by the end of 1998, and start its commissioning period with beams in early 1999.

5. Acknowledgments

The work reported in this paper has been carried out by many individuals, too numerous to list. There are large teams at the three laboratories, SLAC, LBL and LLNL, carrying out the machine design and construction. A far greater number of institutions are involved in the design of the detector worldwide.

6. References

1. *PEP II - An Asymmetric B-Factory Conceptual Design Report,* LBL PUB 5379, SLAC-418, June 1993.
2. *Letter of Intent for the Study of CP Violation and Heavy Flavor Physics at PEP II*, SLAC-443, June 1994.

LAWRENCE BERKELEY NATIONAL LABORATORY
UNIVERSITY OF CALIFORNIA
TECHNICAL & ELECTRONIC INFORMATION DEPARTMENT
BERKELEY, CALIFORNIA 94720